# High-Temperature Molecular Dynamics Simulation of Cellobiose and Maltose

**Jessica D. Murillo**
Dept. of Chemistry, Tennessee Technological University, Cookeville, TN

College of Interdisciplinary Studies, Environmental Sciences, Tennessee Technological University, Cookeville, TN

**Melissa Moffet**
Dept. of Civil and Environmental Engineering, Tennessee Technological University, Cookeville, TN

**Joseph J. Biernacki**
Dept. of Chemical Engineering, Tennessee Technological University, Cookeville, TN

**Scott Northrup**
Dept. of Chemistry, Tennessee Technological University, Cookeville, TN

*DOI 10.1002/aic.14854*
*Published online May 7, 2015 in Wiley Online Library (wileyonlinelibrary.com)*

*Thermochemical conversion of lignocellulosic biomass to renewable fuels and chemicals occurs through high temperature decomposition of the main structural components in plants, including cellulose, hemicellulose, and lignin. Cellulose and hemicellulose comprise mostly carbohydrates. Two disaccharides, maltose and cellobiose, are used as model compounds to explore differences in thermal stability due to the orientation of the glycosidic bond. First principles molecular dynamics and density functional theory have been used to probe the decomposition of these disaccharides during pyrolysis at 700 K. The results suggest that maltose, the α-disaccharide, is less thermally stable. Dynamic bond length analysis for maltose indicates that several C—C bonds and the C—O bonds on the pyranose ring demonstrate signs of weakening, whereas no such scissile bonds were identified for cellobiose. The higher stability of the cellobiose is believed to originate from the persistence of low-energy hydroxymethyl conformers throughout the simulation which enable strong inter-ring hydrogen bonding. Thermogravimetric and mass spectroscopic experiments corroborate the enhanced thermal stability of cellobiose, wherein the onset of decomposition was observed at higher temperatures for cellobiose than for maltose.* © 2015 American Institute of Chemical Engineers *AIChE J*, 61: 2562–2570, 2015
*Keywords: molecular dynamics, high temperature, kinetics, cellobiose, maltose*

## Introduction

Mono-saccharides and disaccharides have been extensively studied as model compounds for more complex carbohydrates such as cellulose as cellulose has received much attention as the primary reactant in the conversion of plant material to fuels via chemical and thermal processes. Biomass pyrolysis, in particular, is the thermal decomposition of organic materials at high temperature in an inert atmosphere. Pyrolysis of biomass is capable of producing liquid and gaseous products that can be upgraded to a variety of fuels and specialty chemicals. To study the fundamental mechanisms leading to the major pyrolysis products, computational methods capable of capturing bond breaking and bond forming events are sought. Within the computational chemistry literature, the majority of the work has been focused on the conformational and dynamical properties of carbohydrates in solvent.[1–6] Many of these studies have tested the utility of large basis sets for geometry optimizations and energy calculations and advanced levels of theory have been used for a variety of solvated carbohydrate systems. The purpose of this study is to investigate differences in thermal stability between the α- and β-linked disaccharides, maltose, and cellobiose, using first principles molecular dynamics (MD) simulations at high-temperature to identify potential bond cleavage sites and hydrogen bonding patterns *in vacuo*. However, no computational studies directly related to pyrolysis or thermal stability of cellobiose and maltose could be found.

Using *ab initio* Car–Parinello molecular dynamics (CPMD) and metadynamics (an accelerated MD technique) simulations of crystalline cellulose pyrolysis, Agarwal et al.[7] suggests precursor pathways for formation of formic acid, 5-hydroxy methyl furfural (5-HMFU), and levoglucosan (LVG), three major products of cellulose pyrolysis. At the same time, α-cyclodextrin (ACD) has been proposed as a surrogate compound for the pyrolysis of cellulose.[8] Its smaller size (lower molecular weight) makes it amenable to longer and more complex MD calculations than if whole cellulose is modeled.

Correspondence concerning this article should be addressed to J. J. Biernacki at jbiernacki@tntech.edu.

CPMD simulations of ACD suggest reaction mechanisms for major pyrolysis products such as furans, glycoaldehyde, formic acid, CO, and $CO_2$ via concerted homolytic cleavage of the glycosidic and pyran ring bond.[8] This approach, however, assumes that $\alpha$- and $\beta$-carbohydrates behave the same, mechanistically and kinetically, at high temperatures. Mettler et al.,[8] emphasize that furans and other products form directly from cellulose (or in this case, ACD) without going through any small-molecule intermediates (e.g., glucose and LVG). Moreover, previously hypothesized heterolytic reaction mechanisms are contested elsewhere.[9] Although, there are many molecular simulation-based studies that address conformation distributions and energetics of small carbohydrates at the ground state, much less is found in the literature on the high-temperature behavior of carbohydrates; and very few articles focus on the reactive sites and relative bond stabilities of saccharide anomers at pyrolysis conditions. For that matter, side-by-side experimental datasets for anomer pyrolysis are almost nonexistent. However, in a well-documented, but brief work by Pavlath and Gregorski,[10] they provide a rare side-by-side comparison of the thermal stability of cellobiose and maltose that suggests that the $\alpha$-bonded anomer (maltose) is somewhat less stable, that is, has a lower decomposition threshold. Having compared the thermal stability for other anomeric disaccharides as well, they concluded that "it appears... that beta-couplings increase the pyrolitic stability of disaccharides... ." Hence, the present study aims to supplement these findings with computational outcomes and new experimental datasets in an attempt to validate or invalidate this hypothesis for the glucose-based disaccharides cellobiose and maltose.

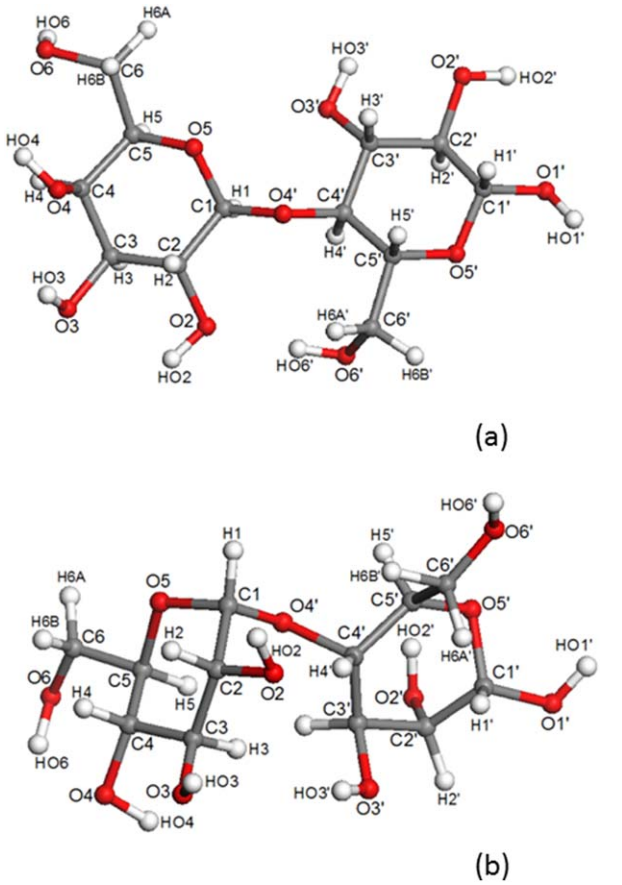


**Figure 1. Structure and nomenclature for cellobiose (a) and maltose (b).**

**[Color figure can be viewed in the online issue, which is available at wileyonlinelibrary.com.]**

## Computational Method

### *Nomenclature and starting structures*

The structure of maltose and cellobiose are shown in Figure 1. Atoms are labeled with the standard numbering scheme of carbohydrates. Atoms on the reducing glucose residue are designated with a primed label, and the nonreducing ring atoms are shown unprimed. The glucose ring with the hydroxyl group at C1 is called the reducing end because in the open-ring form it can participate in redox reactions, whereas the glucose ring with a hydroxyl group at C4 is called the nonreducing ring. Initial coordinates for cellobiose were obtained from the cellulose crystallographic information file provided by Nishiyama et al.[11] A cellobiose dimer, the repeating unit within the cellulose crystal lattice, was extracted, optimized, and used for MD simulations. Similarly for maltose, initial coordinates were imported from an x-ray diffraction (XRD) experimental dataset.[12]

### *Software and geometry optimization*

Three-dimensional representations of cellobiose and maltose were obtained by importing the initial coordinates into the Accelrys Materials Studio 5.5 visualizer. Hydrogen atoms were added and the molecule was coarsely optimized using the "Clean" function to obtain a lower energy starting structure for further refinement. All subsequent energy optimizations and MD simulations were performed in the DMol3 module using the Kohn–Sham[13,14] formulation of density functional theory (DFT). The gradient-corrected exchange-correlation functional of Becke[15] and Lee–Yang–Parr[16] was used to calculate the DFT electronic energy for each all-electron system. A numerical basis set was used to expand the Kohn–Sham orbitals. The double numerical polarization (DNP) basis set available within the DMol3 module was used with basis set file version 4.4.[17] The DNP basis set offers one atomic orbital for each occupied atomic orbital and a second set of valence atomic orbitals, in addition to d- and p-polarization functions for non-hydrogen and hydrogen atoms, respectively. Initial geometry optimizations were performed for each molecule using the "coarse" setting which automatically designates the self-consistent field (SCF) convergence to $1 \times 10^{-4}$ and the integration grid to the "coarse" setting. This step diminished the time required to optimize the structures further using the "fine" electronic and integration setting (SCF = $1 \times 10^{-6}$).

### *Molecular dynamics*

MD simulations in DMol3 are based on the velocity Verlet[18,19] algorithm for the integration of the equations of motion. Simulations were performed with the canonical ensemble, constant moles, volume and temperature (NVT), maintained at 700 K using the Nosé–Hoover[20] chain thermostat with a chain length of 4.0 and a Nosé ratio of 1.0 to scale the fictitious mass, $Q$, which determines the feedback rate between the instantaneous kinetic energy and the required temperature. The default value of 3.0 was used for the Yoshida–Suzuki[21–23] integration parameter of the velocity Verlet algorithm. Minimized coordinates from geometry optimized structures as described above were used to start the

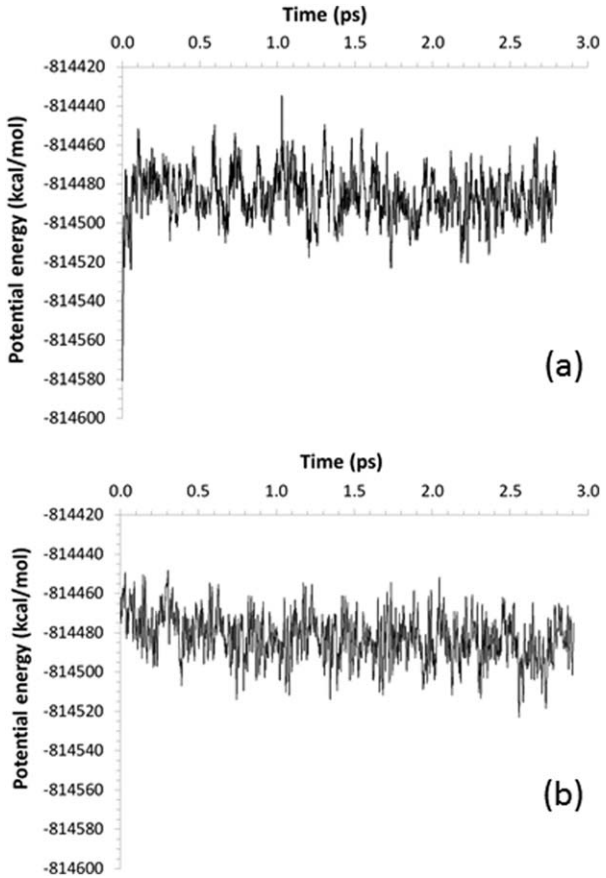


**Figure 2. Potential energy curves of cellobiose (a) and maltose (b) for a 3-ps MD simulation at 700 K.**

MD simulations. Initial velocities were assigned for each atom in the molecule from a Maxwell–Boltzman distribution. A time step of 0.12 fs was implemented for a total of 24,000 time steps and a simulation period of about 3 ps.

### *Thermogravimetry-mass spectrometry*

A TA Instruments SDT Q600 Simultaneous differential scanning calorimeter-thermal gravimetric analyzer (DSC-TGA) was used in this study. Approximately 20 mg samples of cellobiose or maltose were distributed evenly in an open top alumina crucible. Using a gas flow rate of 50 mL/min, ultrahigh purity argon was used to purge the furnace of oxygen at 27°C for 120 min which was then ramped to 1000°C using a linear heating rate of 10 °C/min.

An unheated transfer line connected the thermogravimetric analysis (TGA) furnace to the mass spectrometer for evolved gas analysis. While condensable organic compounds could not be measured using this thermogravimetry-mass spectrometry (TG-MS) setup, permanent gases from the decomposition of cellulose and maltose were detected using a Monitor Instruments MG 2100 Gas Analyzer. Single ion monitoring (SIM) was used to track peaks at m/z 2, 16, 18, 28, and 44, where each mass is postulated to be a good indicator in the detection of $H_2$, $CH_4$, $H_2O$, CO, and $CO_2$, respectively. Mass spectra were obtained in electron impact mode (2.00 ev).

## Results and Discussion

Time as a function of total potential energy for cellobiose and maltose are shown in Figures 2a, b, respectively. The graphs indicate that soon after the start of simulation the potential energy oscillates around a steady value of −814,483 kcal/mol for cellobiose and −814,476 kcal/mol for maltose over the entire simulation time. These values are very similar to the *in vacuo* DFT values for the relative energies with respect to the lowest energy minimum of cellobiose (−814,487.69 kcal/mol)[24] and maltose (−814,728.07 kcal/mol).[25] Between thermostatic resetting, the total energy was conserved. The thermostat introduced small fluctuations of ±0.3 kcal/mol per degree of freedom indicating a thorough equipartitioning of energy in all degrees of freedom. In lieu of ideal long equilibration times, the observed constant energy and stable temperature at about 700 K were taken as evidence of a stabilized, physically representative system. Even when long integration time periods are implemented it is difficult to know when thermodynamic equilibrium has been reached. In addition, MD simulations require very small, computationally expensive integration time steps, usually much smaller than 1 fs, and are restricted to simulation periods of 10–100 ps,[7] with the higher end of the range restricted to supercomputers. With the available computer technology in a standard research facility, a simulation period of 10–50 ps, the lower end of the range, is more practical for MD simulations in terms of computational resources.

Carbohydrates present a particularly difficult problem in molecular modeling. The conformational freedom and the donor and acceptor property of the many —OH groups in carbohydrate structures leads to a multiplicity of local minima of nearly equal energy.[26] The atoms defining the calculated dihedral angles for cellobiose and maltose are shown in Figure 3. MD trajectories for $\varphi$, and $\psi$, are shown in Figures 4 and 5

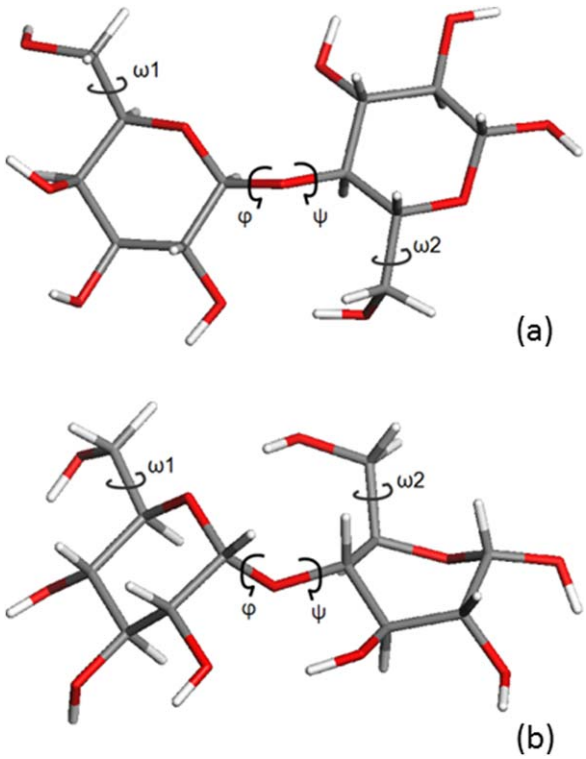


**Figure 3. Torsion angles monitored for cellobiose (a) and maltose (b).**

**[Color figure can be viewed in the online issue, which is available at wileyonlinelibrary.com.]**

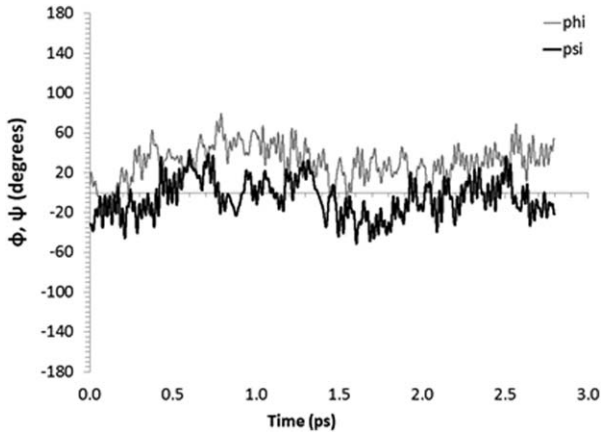


**Figure 4. Dihedral angle, $\varphi$ = H1—C1—O4′—C4′ and $\psi$ = C1—O4′—C4′—H4′ for cellobiose.**

for cellobiose and maltose, respectively. Dihedral angles for the cellobiose structure at the start of the simulation are approximately ($\varphi$, $\psi$) $\sim$ (20°, −40°), which represents one of five energy minima obtained from total energy surface calculated for an uncharged cellobiose molecule.[27] Torsion angles for maltose start at ($\varphi$, $\psi$) $\sim$ (−20°, −5°), which still fall within the low-energy valley described by Hardy and Sarko along a $\varphi$ angle of $30 \pm 20°$ and extending in $\psi$ from 180 to −180°.[27] Recently, Strati et al. performed *in vacuo* DFT/*ab initio* calculations using a 6-311++G** basis set and found that a "flipped" conformer of cellobiose where $\varphi \approx 180°$ is the most stable structure, and not the experimentally found conformer with dihedral values in the range of ($\varphi$, $\psi$) $\sim$ (40°, −20°).[28] The same "flipped" conformer was found by Hardy and Sarko as one of two higher-energy minima located away from the aforementioned low-energy valley on the potential energy map of cellobiose.

### *Hydroxymethyl conformers of maltose and cellobiose*

The hydroxymethyl group at C6 has three low-energy rotameric conformers assigned a two-letter name according to the *trans* or *gauche* dihedral relationship with the ring oxygen O5—C5—C6—O6. The $\omega$ rotation angle is 0° when C4—C5—C6—O6 or C4′—C5′—C6′—O6′ is cis. The exocyclic torsion angle position *gt* is equivalent to 180°, *gg* is 60°, and *tg* equals −60°.[28] MD trajectories for $\omega$1 and $\omega$2 are shown in Figure 6, where $\omega$1 and $\omega$2 designate the rotation about the C5—C6, and C5′—C6′ bond, respectively. The hydroxymethyl on the nonreducing ring of cellobiose maintains a *gg* conformation for over half of the simulation and then transitions to *tg* rotamer. The hydroxymethyl group on the reducing ring shows more activity as it alternates between *tg* and *gt* throughout the simulation. Experiment indicates that *gg* and *gt* have the lowest and almost equal energy (within ±0.2 kcal/mol), while the *tg* conformation is less favored by 1.4 kcal/mol for the $\beta$-anomer and 2.2 kcal/mol for the $\alpha$-anomer.[27] This trend was found to be true in solvent and *in vacuo*. The hydroxymethyl group on the nonreducing ring of maltose remains in the high energy *tg* conformer for the entire simulation, while the hydroxymethyl group on the reducing glucose residue is able to quickly transition from *tg* conformation at the start of the simulation to the lower energy *gt* conformer, where it remains 83% of the time. These conformational changes give insight into the relative differences in stability at high temperatures for the two disaccharides. For both disaccharides, the nonreducing residue maintained a long-lived conformer: for cellobiose, the hydroxymethyl group nonreducing monosaccharide of cellobiose molecule retains the low-energy *gg* rotamer was present 66% of the time, while for maltose the hydroxymethyl remained in the high energy *tg* conformer for the entire simulation. Conversely, the hydroxymethyl group on reducing rings demonstrated five total transitions for both

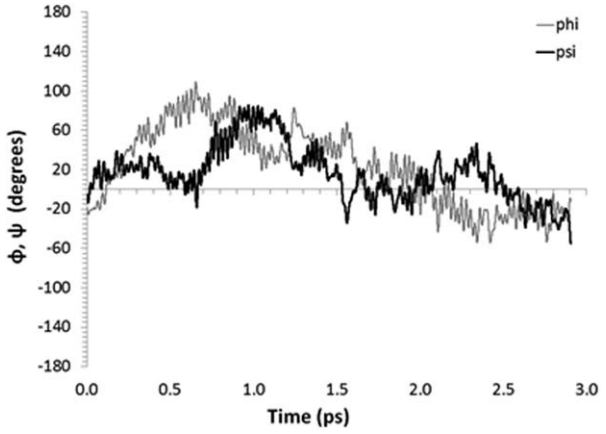


**Figure 5. Dihedral angle, $\varphi$ = H1—C1—O4′—C4′ and $\psi$ = C1—O4′—C4′—H4′ for maltose.**

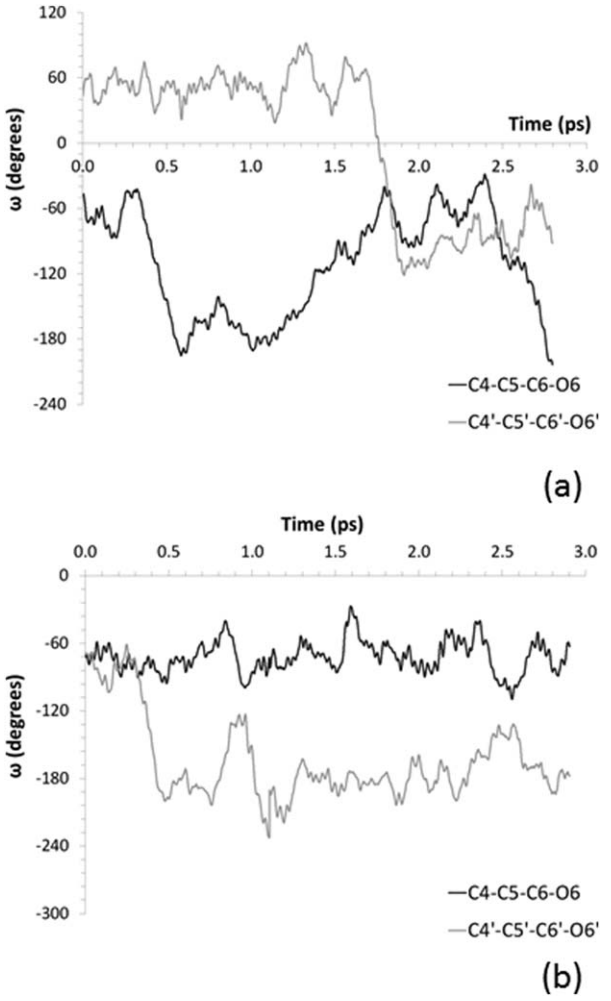


**Figure 6. Dihedral angles for the hydroxymethyl groups in cellobiose (a) and maltose (b).**

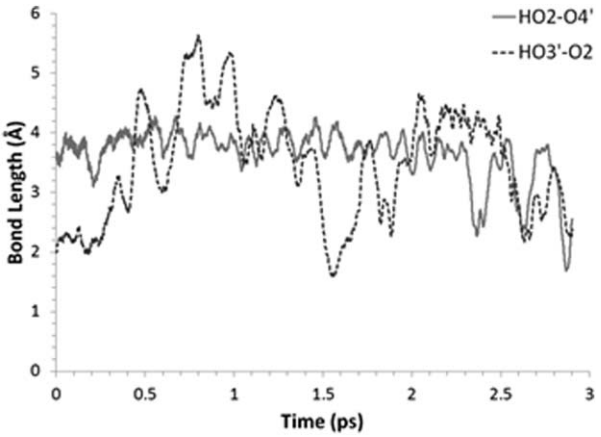


**Figure 7. Inter-ring hydrogen bonds for maltose during a 3-ps MD run.**

disaccharides. The high temperature simulation selected for this simulation inputs the required energy to overcome energy barrier between the *tg*:*gt* conformers within a smaller simulation window. The energy barriers between *gt* and *tg* are about 12 kJ/mol and approximately eight transitions can be observed within 1 ns at 300 K.[29]

### *Intraring and Inter-ring hydrogen bonding patterns of maltose and cellobiose in vacuo*

Hydrogen bonding is known to affect carbohydrate conformation and stability. Structures of disaccharides can be classified in terms of favored orientation of the hydroxymethyl side chain, as discussed above, and by the orientation of the pendant alcohol groups on the sugar rings as clockwise (c) or counterclockwise (r).[27] Figure 1a shows a good example of the c orientation of the exocyclic hydroxyl groups around each glucose residue in the cellobiose structure. This orientation facilitates hydrogen bonding between HO4 and the hydroxymethyl oxygen atom, O6. Both disaccharides exhibit extensive intraring hydrogen bonds. Intraring hydrogen bonds on the reducing ring of maltose and on the nonreducing ring of cellobiose are persistent throughout the simulation. In maltose, single and bifurcated hydrogen bonds were observed between HO1′···O2′, HO2′···O1′, HO2′···O3′, HO2′···O5′, and HO6′···O5′. The higher frequency of strong hydrogen bonds on the reducing ring is likely due to the fact that the hydroxymethyl group on this ring oscillates around the more stable *gt* conformer which enables the formation of these bonds. Maltose shows a different trend on the nonreducing ring, where only three short-lived hydrogen bonds between HO2′···O3′, HO4′···O3′, and HO4′···O6′ are detected.

The nonreducing glucose ring of cellobiose is maintained in the low-energy *gg* hydroxymethyl conformer which enables the formation of six hydrogen bond interactions, HO3···O2, HO3···O4, HO4···O3, HO4···O5, HO6···O4, and HO6···O5, all of which reach a hydrogen bond length of less than 2.0 Å. At about 1.8 ps, a transition in conformation occurs from *gg* to *tg* and the intraring hydrogen bonding scheme is disrupted. Of the four intraring (between atoms on a single glucose residue) hydrogen bonds observed on the reducing ring of cellobiose, HO1′···O2′, HO2′···O1′, HO2′···O3′, HO6′···O5′, only the interactions observe between HO6′···O5′ and HO2′···O1′ show strong bonding (i.e., reaching small bonding distances). Intraring hydrogen bonds were found to be more stable than inter-ring hydrogen bonds during the slow heating of cellulose.[30] However, the difference in the number of inter-ring hydrogen bonds contributes to the overall thermal stability of these disaccharides.

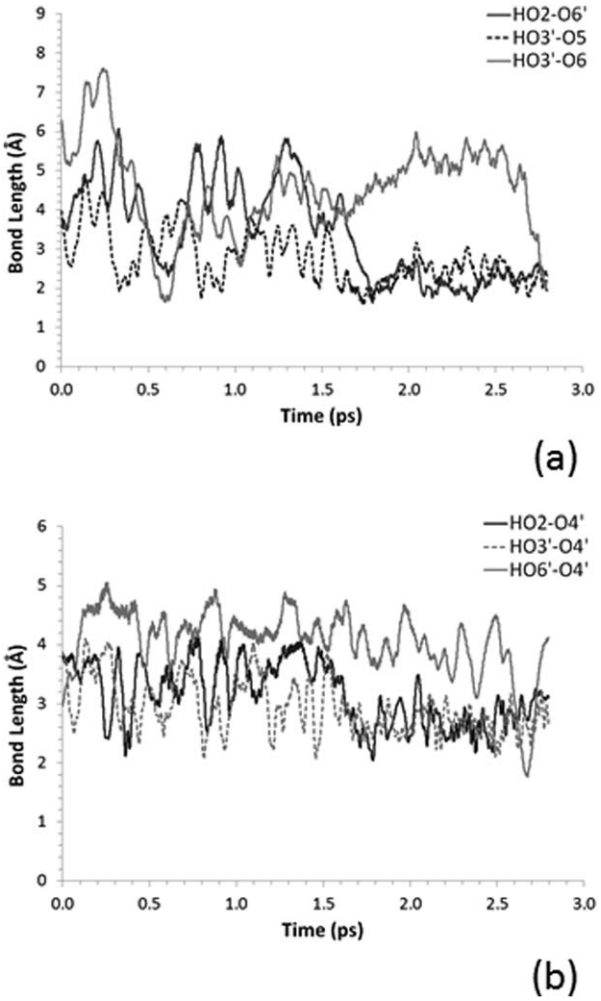


**Figure 8. Observed hydrogen bonds for cellobiose during a 3ps MD run involving inter-ring bonds (a) and bridge oxygen, O4′ (b).**

Inter-ring hydrogen bonds are shown in Figure 7 for maltose and in Figure 8 for cellobiose. It is clear that more inter-ring bonding is observed for the $\beta$-disaccharide. Maltose shows two inter-ring interactions: one where HO3′ on the reducing ring bonds to the O2 atom of the nonreducing ring, and another event where HO2 is bonded to the bridging oxygen, O4′. The latter bond demonstrates strong bonding throughout the entire simulation, while the HO3′···O2 interaction is intermittently active toward the end of the simulation.

Inter-ring hydrogen bonds for cellobiose are graphed separately for clarity. Figure 8a shows interactions between glucose residues and Figure 8b shows hydrogen bonds involving the bridging oxygen. Even with a cutoff of 2.5 Å, strong hydrogen bond interactions are maintained throughout the entire simulation period. Around 2.0 ps, bifurcated hydrogen bonds originating at HO2 and HO3′ each form one bond with the glycosyl oxygen (O4′) and with one atom from the opposite glucose residue, O6′ and O5, respectively. This forms a cooperative network that stabilizes the structure, and more importantly, is not observed for maltose to

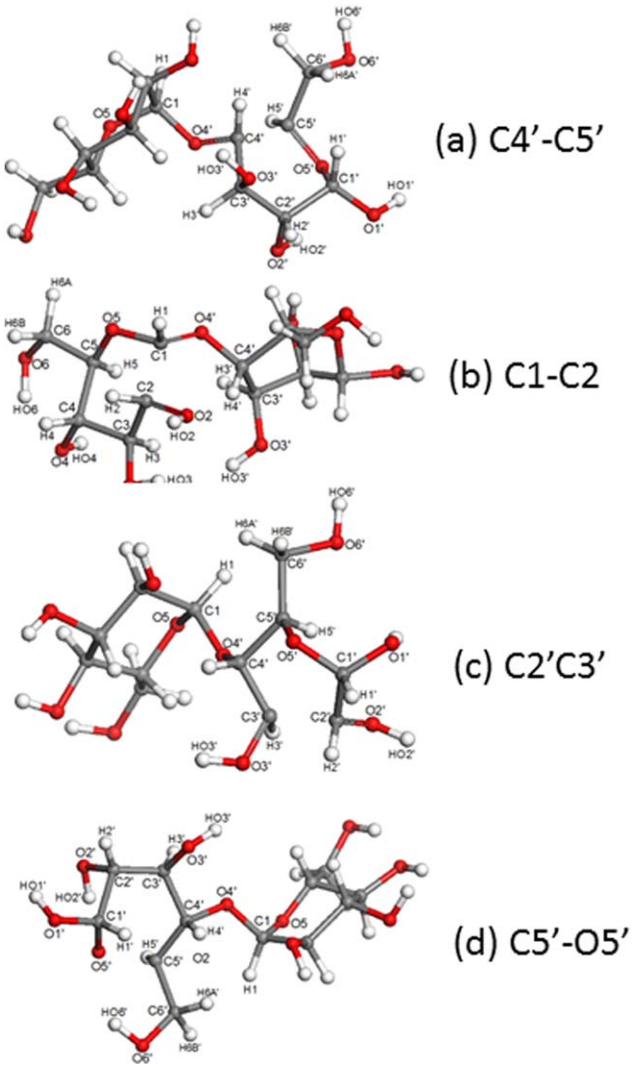


**Figure 9. Weak bonds at C4′—C5′ (a), C1—C2 (b), C2′—C3′ (c), C5′—O5′(d) on the α-disaccharide, maltose, during a 3-ps MD simulation at 700 K.**

**[Color figure can be viewed in the online issue, which is available at wileyonlinelibrary.com.]**

any extent. In fact, the HO2′···O6 and HO3···O6′ have been shown to exist in modeling studies of cellulose, with the former donor–acceptor pair being the most stable interchain hydrogen bond due to its stability at low and high temperatures.[31] It is hypothesized that deficiencies in the inter-ring hydrogen bond network of maltose is, in part, responsible for several observed weakened bonds and potential reactive sites.

### *Bond length analysis of maltose*

Figure 9 shows the bonds that stretched far from equilibrium bond length during the MD simulation for the α-disaccharide, maltose. No comparable bond lengthening events were observed for cellobiose. At 0.58 ps, the C4′—C5′ bond of maltose exhibits an root mean squared (RMS) deviation of 0.06 (averaged over the entire duration of the bond-breaking event) from its equilibrium bond length of 1.55 Å (Figure 10). This might suggest a reactive center where the C4′ on the reducing ring forms a double bond

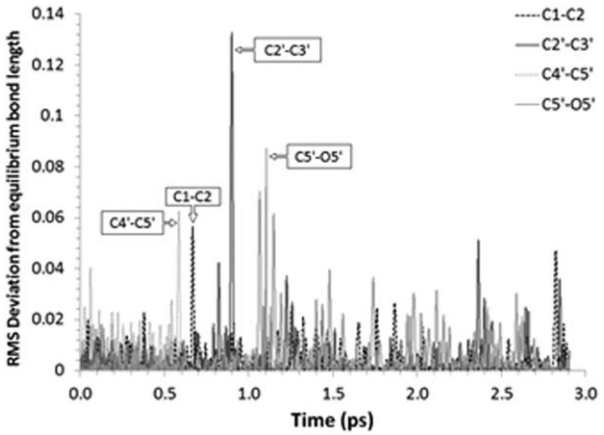


**Figure 10. RMS deviations from equilibrium bonds lengths for maltose during MD simulation.**

with the bridge oxygen O4′, while C5′ forms a double bond with the pyran ring oxygen, O5′. This structure is shown in Figure 9a. The maximum distance observed between C4′ and C5′ is about 1.8 Å (Figure 11), while the newly formed C4′═O4′ bond shrinks to about 1.37 Å. As default values for monitoring bond distances are useful only for visualizing atomic interactions during the simulations with the DMol3 module, the freeware MultiWFN Analyzer 3.0[32] was used to perform a topological electron density analysis. Electron density analysis was performed to determine the strength of bond for atoms that showed large perturbations from equilibrium bonding distance (Figures 9a–d).

MultiWFN uses principles from the quantum theory of atoms-in-a-molecule (QTAIM) to unambiguously define bonding between two atoms.[33] According to QTAIM, the bond path is a single line of locally maximum density linking the nuclei of two bonded atoms, and thus is a universal indicator of all types of chemical bonds (e.g., weak, strong, open, and closed shell).[33] The point on the bond path with the lowest value of the electron density is the bond critical path (BCP). The collection of bond paths linking the nuclei of bonded atoms in a molecule is called the molecular graph, or atomic interaction lines for nonequilibrium geometries, which can be used to locate changes in structure along a reaction path.[33] These calculations were performed on the wavefunction of the maltose structures shown in Figure 9 to

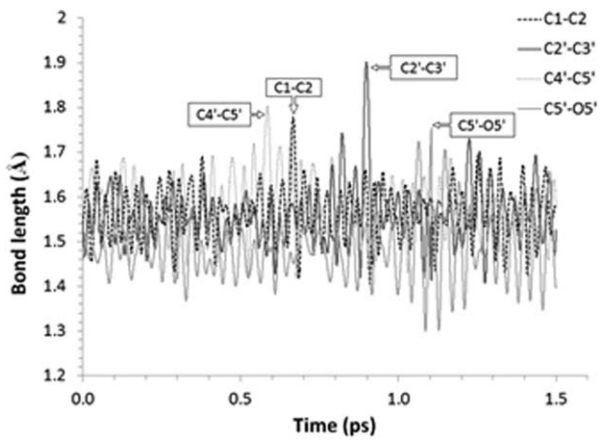


**Figure 11. Selected bonds in maltose showing bond stretching during MD simulation.**

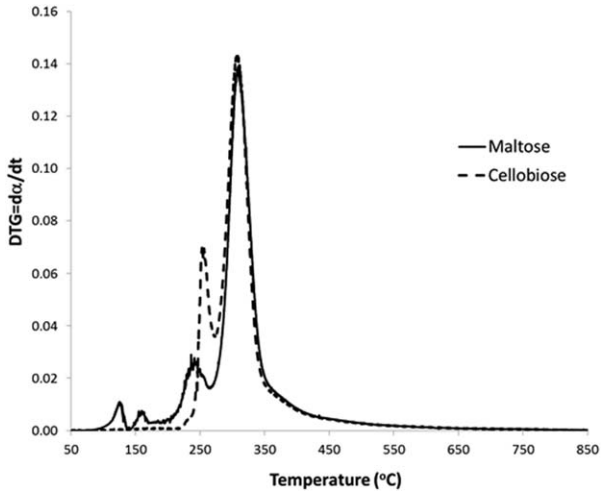


**Figure 12. DTG curves for maltose and cellobiose.**

analyze the interactions between the atoms with potential scissile bonds. Low electron density values on the order of $1 \times 10^{-3}$ a.u. confirm a weak bond between two atoms. In comparison, electron density at the BCP is greater than 0.20 a.u. in covalent bonds, and less than 0.10 a.u. in closed-shell interactions, such as ionic, van der Waals, and hydrogen bonds.[33]

Figure 9b shows the structure of maltose at 0.66 ps. The nonreducing ring shows weak electron density along the C1—C2 bond, wherein the C1—C2 is weakened. Reactions at this site could involve the formation of a double bond between C2 and the hydroxyl oxygen, O2, while C1 forms a double bond with the bridge oxygen, O4′. In this case, the two double bonds formed do not show a decrease in bond length. Instead, the C2═O2 bond increased slightly to 1.47 Å from its equilibrium bond length of 1.44 Å. The double bond at the bridge oxygen between C1═O4′ changed only slightly (1.40 Å) from its equilibrium bond length of 1.42 Å. The discrepancy in bond length might be explained by considering the bond length of the attached OH group. Strati et al. observed that the varying bond length of the O—H bond in turn affected the C—O bond length, so that when O—H became shorter, the C—O bond is slightly longer, and vice versa.[28] During the elapsed time of this bond stretching event, the OH2—O2 group does not participate in hydrogen bonding and is observed to decrease in bond length by 0.04 Å, from its equilibrium bond length of 0.98 Å.

At approximately 0.89 ps, the C2′—C3′ bond on the reducing ring of maltose, extends from an equilibrium bond length of about 1.45 Å to approximately 1.90 Å. Such perturbation from equilibrium could leave to bond cleavage, wherein each carbon forms a double bond with the corresponding hydroxyl oxygen, O2′ and O3′, respectively. The bond lengths of the new double bonds are about 0.02 Å shorter than the equilibrium bond length of 1.45 and 1.44 Å, for C2′—O2′ and C3′—O3′, respectively. At 1.1 ps, the distance between the C5′ and O5′ atom reach a maximum distance of 1.75 Å, that is, 0.3 Å longer than the equilibrium bond length of 1.46 Å. The pyran ring C5′—O5′ bond could be a reactive site with no accompanying bond formation (Figure 9d). Neighboring bonds C1′—O5′ and C4′—C5′ remained about the same length, changing by no more than 0.03 and 0.01 Å from equilibrium bond length 1.46 and 1.55 Å, respectively. Bond cleavage at the pyran ring C—O bond was found to be a typical reactive center found for the carbohydrate, α-cyclodextrin. High-temperature condensed-phase MD simulation of ACD revealed that mechanistic pathways leading to the formation of furans, formaldehyde, formic acid, and $CO_2$, among other products are initiated by homolytic cleavage of the pyran C—O bond.[8] No weak C—O bond sites were found at the glycosidic bond for either disaccharide during the MD simulation.

### *TG-MS and evolved gas analysis for maltose and cellobiose*

Analytical techniques such as nuclear magnetic resonance (NMR) and XRD are useful for experimental corroboration of the structural phenomena, at the relevant length scale, deduced through computational methods. For the current work, it is crucial to understand the thermal stability and kinetics as a result of structural differences between maltose and cellobiose; however, NMR and XRD do not offer the appropriate platform to test such properties, whereas, TGA is a precise way to measure thermal and kinetic behavior of materials when accompanied by mass changes. Here, bulk thermal analysis is conducted on maltose and cellobiose, while simultaneously analyzing product gases using MS.

The derivative thermal gravimetric (DTG) curves for maltose and cellobiose are shown in Figure 12. The DTG curve for maltose monohydrate shows what appears to be two-step dehydration with an initial peak at 98 °C and a second smaller peak on the DTG curve at about 150 °C. The calculated cumulative weight loss associate with these two peaks closely matches the theoretical weight loss expected for maltose monohydrate of 5.26% (mass/mass). The melted maltose sample remains unchanged until about 205 °C when weight loss of the sugar begins (at ~138 min). The cellobiose is an anhydrous crystalline solid, thus no dehydration peak is observed. A peak corresponding to cellobiose weight loss is observed at 220 °C, which corresponds to other works that report similar behavior at about 225 °C, see Shafizadeh and Lai.[34]

MS was used to confirm that weight loss is indeed associated with decomposition and not just evaporation. The MS was used in SIM mode to scan for masses 2, 16, 18, 28, and 44, where each mass is postulated to be a good indicator in

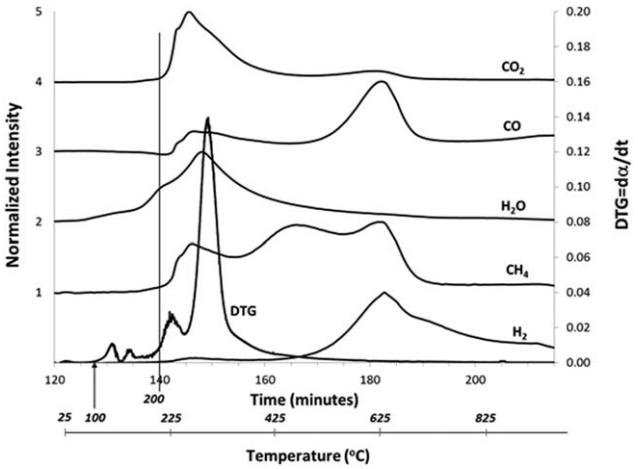


**Figure 13. TG-MS curves of maltose. Two *x* axes are shown, one indicates reaction time and the other pyrolysis temperature.**

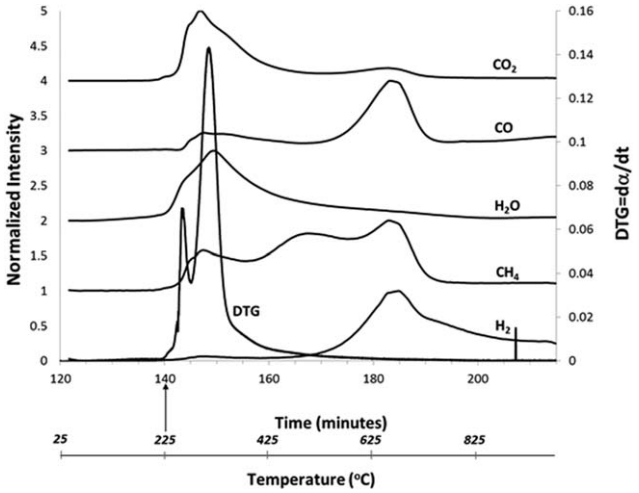


**Figure 14. TG-MS curves of cellobiose. Two *x* axes are shown, one indicates reaction time and the other pyrolysis temperature.**

the detection of $H_2$, $CH_4$, $H_2O$, CO, and $CO_2$, respectively. Although the *m*/*z* values chosen are not unique, when the entire spectrum of pyrolysis products are considered, full scans between *m*/*z* 2–200 revealed that no high molecular weight fragments make it into the MS, that is, not to say that high-molecular weight products are not formed, but rather could not be detected with this experimental setup. Noncondensable gases, such as $H_2$ and $CO_2$ are commonly observed during pyrolysis of carbohydrates and can, however, be used as reliable indicators of decomposition. Figure 13 shows the MS results for maltose overlaid with the TGA data as a function of both time and temperature. Ions at $m/z = 18$ indicate that water is the only species detected between a temperature of about 100 and 150 °C demonstrating conclusively that the two small initial peaks for maltose to be dehydration as expected. Water, carbon dioxide, and mass 16 (which may be methane or an ion fragment of formic acid, acetic acid, or acetaldehyde) all begin to appear immediately as the rate of weight loss increases at about 200 °C (~138 min). The lighter gases such as hydrogen and carbon monoxide appear later, 170 and 182 min, respectively. Water, hydrogen, carbon dioxide, and carbon monoxide are all known decomposition products of sugars.[35] Similarly, *m*/*z* signals for cellobiose (Figure 14) indicate thermal decomposition at the very onset of weight loss at about 225 °C (140 min). In the case of cellobiose, however, thermal decomposition is not preceded by dehydration as the parent material is already anhydrous.

## Conclusion

The dynamic behavior of cellobiose and maltose was studied by MD simulations at 700 K. The disaccharides transition between different conformers throughout the 3-ps simulation period. Rotameric conformations about the C5—C6 bond of each glucose residue are believed to contribute to differences in thermal stability observed between the α- and β-disaccharide. Low energy conformers (*gg* and *gt*) facilitate the extensive and persistent intraring and interring hydrogen bond network in cellobiose. Maltose, however, showed less persistent inter-ring hydrogen bonding. Differences in inter-ring hydrogen bonds are suggested to play a role in the superior thermal stability of the β-disaccharide over the α-disaccharide. Only two inter-ring hydrogen bond events were observed for maltose, and in addition to being sparse, these interactions were short-lived. Cellobiose demonstrated six different hydrogen bonds that maintained relatively strong interactions throughout the simulation.

Maltose exhibits several bonds that stretch far beyond equilibrium lengths, suggesting that these are potential reactive sites, likely due, in part, to the lack of inter-ring stability when compared to the cellobiose structure. Reactive sites include C—C ring bonds, two on the reducing ring and one on the nonreducing ring, as well as the C—O bond on the reducing ring of maltose. Early researchers have found that similar bond energies can be assigned to all C—C and C—O bonds, interatomic distances change slightly for C2—C3 bond, and the C1—O1 bond on the pyran ring making these positions initial reactive sites for subsequent reactions to take place and to form a variety of low molecular weight compounds.[36] If the number of weakened bond sites is any indication of thermal stability, then the results presented here would have implications on thermal processing of carbohydrates, such as in the pyrolysis of cellulosic material. Results show that the majority of ring opening reactions might occur through an initial C—C bond cleavage step rather than cleavage at the pyran ring or bridging C—O bond as suggested by implied simulations of cellulose decomposition with MD simulations of an α-linked model compound.[8] Undoubtedly, longer simulations are required to provide conclusive evidence of differences in high-temperature behavior between the two anomers. Experimental results using TG-MS conclusively show that maltose begins decomposition at lower temperatures than the anomeric β-bonded saccharide. Additionally, decomposition products including $CO_2$ formed after the onset of weight loss show that weight loss is not simply due to evaporation of the parent saccharide. TGA results also indicate that although it is possible for the α and β carbohydrate anomers studied here to form the same products, the kinetic pathways, and likely the mechanisms, by which they occur are likely different putting into question the utility of using α-bonded surrogate compounds for implying kinetic transformations about cellulose pyrolysis.

## Acknowledgments

JDM would like to thank Michael Renfro for his assistance with data processing throughout the project. Thanks to Lasantha Rathnayake for his help with the QTAIM and MultiWFN analysis and for his helpful discussions. The authors also acknowledge financial support from the National Science Foundation (NSF) through Grant Award No. CBET-1360703.

## Literature Cited

1. Pereira CS, Kony D, Baron R, Müller M, van Gunsteren WF, Hünenberger PH. Conformational and dynamical properties of disaccharides in water: a molecular dynamics study. *Biophys J*. 2006;90:4337–4344.
2. Patel DS, Pendrill R, Mallajosyula SS, Widmalm G, MacKerell AD Jr. Conformational properties of a or b-(1→6)-linked oligosaccharides: Hamiltonian replica exchange MD simulations and NMR experiments. *J Phys Chem B*. 2014;118(11):2851–2871.
3. Apell M, Strati GL, Willett JL, Momany FA. B3LYP/6-311++G** study of α- and β-D-glucopyranose and 1,5-anhydro-D-glucitol: $^4C_1$ and $^1C_4$ chairs, $^{3,O}B$ and $B_{3,O}$ boats, and skew-boat conformations. *Carbohydr Res*. 2004;339:537–551.

4. Apell M, Willett JL, Momany FA. DFT study of α- and β-D-mannopyranose at the B3LYP/6_311++ G** level. *Carbohydr Res*. 2005;340:459–468.
5. Momany FA, Apell M, Willett JL, Bosma WB. B3LYP/6_311++ G** geometry-optimization study of pentahydrates of α- and β-D-glucopyranose. *Carbohydr Res*. 2005;340:1638–1655.
6. Momany FA, Apell M, Willett JL, Schnupf U, Bosma WB. DFT study of α- and β-D-galactopyranose at the B3LYP/6_311++ G** level of theory. *Carbohydr Res*. 2006;341:525–537.
7. Agarwal V, Dauenhauer PJ, Huber GW, Auerbach SM. Ab initio dynamics of cellulose pyrolysis: nascent decomposition pathways at 327 and 600° C. *J Am Chem Soc*. 2012;134:14958–14972.
8. Mettler MS, Paulsen AD, Vlachos DG, Dauenhauer PJ. Pyrolytic conversion of cellulose to fuels: levoglucosan deoxygenation via eleimination and cyclization within molten biomass. *Energy Environ Sci*. 2012;5:7864–7878.
9. Varhegyi G, Antal MJ Jr., Szekely T, Till F, Jakab E. Simultaneous thermogravometric-mass spectrometric studies of the thermal decomposition of biopolymers. 1. Avicel cellulose in the presence and absence of catalysts. *Energy Fuels*. 1988;2:267–272.
10. Pavlath AE, Gregorski KS. *Fundamentals of Thermochemical Biomass Conversion*. In: Overend RP, Milne TA, Mudge LK, editors. London: Elsevier Applied Science Publishers, 1985:472–452.
11. Nishiyama Y, Langan P, Chanzy H. Crystal structure and hydrogen-bonding system and cellulose 1β from synchrotron X-ray and neutron fiber diffraction. *J Am Chem Soc*. 2002;124:9074–9082.
12. Santos CR, Meza AN, Paiva JH, Silva JC, Ruller R, Prade RA, Squina FM, Murakami MT. Structure of the hyperthermostable endo-1,4-beta-D-mannanase from thermotoga petrophilia RKU-1 in complex with three maltose molecules. *Protein Data Bank* 2011. DOI:10.2210/pdb3pzo/pdb.
13. Kohn W, Sham LJ. Self-consistent equations including exchange and correlation effects. *Phys Rev*. 1965;140:A1133–A1138.
14. Hohenberg P, Kohn W. Inhomogeneous electron gas. *Phys Rev*. 1964;136:B864–B871.
15. Becke AD. Density-functional thermochemistry. III. The role of exact exchange. *Chem Phys*. 1993;98:5648–5652.
16. Lee C, Yang W, Parr RG. Development of the Colle-Salvetti correlation-energy formula into a functional of the electron density. *Phys Rev B*. 1988;37:785–789.
17. Delley B. Ground-state enthalpies: evaluation of electronic structure approaches with emphasis on the density functional method. *J Phys Chem A*. 2006;110:13632–13639.
18. Verlet L. Computer "experiments" on classical fluids, I. Thermodynamical properties of Lennard-Jones molecules. *Phys Rev*. 1967;159:98–103.
19. Verlet L. Computer "experiments" on classical fluids, II. Thermodynamical properties of Lennard-Jones molecules. *Phys Rev*. 1967;165:201–214.
20. Tuckerman ME, Liu Y, Ciccotti G, Martyna GJ. Non-Hamiltonian molecular dynamics: generalizing Hamiltonian phase space principles to non-Hamiltonian systems. *J Chem Phys*. 2001;115:1678–1702.
21. Yoshida H. Construction of higher order symplectic integrators. *Phys Lett A*. 1990;150:262–268.
22. Suzuki MJ. General theory of fractal path integrals with applications to many-body theories and statistical physics. *J Math Phys*. 1991;32:400–407.
23. Tuckerman ME, Liu Y. Generalized Gaussian moment thermostatting: a new continuous dynamical approach to the canonical ensemble. *J Chem Phys*. 2000;112:1685–1700.
24. Schnupf U, Momany FA. Rapidly calculated DFT relaxed isopotential $\phi/\psi$ maps: β-cellobiose. *Cellulose*. 2011;18:859–887.
25. Momany FA, Schnupf U, Willett JL, Bosma WB. DFT study of α-maltose: influence of hydroxyl orientations on the glycosidic bond. *Struct Chem*. 2007;18:611–632.
26. Jeffrey GA. Experimental and theoretical bases for accurate modeling: an experimentalist looks at modeling. In: French AD, Brady JW, editors. *Computer Modeling of Carbohydrate Molecules*. ACS Symposium Series, Chapter 2. American Chemical Society Symposium Series, 2009;430:20–30.
27. Hardy BJ, Sarko A. Conformational analysis and molecular dynamics simulation of cellobiose and larger cellooligomers. *J Comput Chem*. 1993;14:831–847.
28. Strati GL, Willett JL, Momany FA. Ab initio computational study of β-cellobiose conformers using B3LYP/6-311++G**. *Carbohydr Res*. 2002;337:1833–1849.
29. Ott K-H, Meyer B. Molecular dynamics simulations of maltose in water. *Carbohydr Res*. 1996;281:11–34.
30. Gross AS, Chu J-W. On the molecular origins of biomass recalcitrance: the interaction network and solvation structures of cellulose microfibrils. *J Phys Chem B*. 2010;114:13333–13341.
31. Shen T, Gnanakaran S. The stability of cellulose: a statistical perspective from a coarse-grained model of hydrogen-bond networks. *Biophys J*. 2009;96:3032–3040.
32. Lu T, Chen F. Multiwfn: a multifunctional wavefunction analyzer. *J Comput Chem*. 2012;33:580–592.
33. Matta CF, Boyd RJ, editors. *An introduction to the quantum theory of atoms in molecules (QTAIM). The Quantum Theory of Atoms in a Molecule: From Solid State to DNA and Drug Design*. Chapter 1. Weinheim: Wiley-VCH Verlag GmbH & Co., 2007:1.
34. Shafizadeh F, Lai YZ. Thermal rearrangements of cellobiose and trehalose. *Carbohydr Res*. 1973;31:57–67.
35. Fagerson IS. Thermal degredation of carbohydrates; a review. *J Agric Food Chem*. 1969;17:747–750.
36. Piskorz J, Radlein D, Scott DS. On the mechanism of the rapid pyrolysis of cellulose. *J Anal Appl Pyrol*. 1986;9:121–137.

*Manuscript received Sep. 8, 2014*